Enhanced third harmonic generation by organic materials on high-Q plasmonic photonic crystals

Fanghui Ren,[1] Xiangyu Wang,[1] Zhong'an Li,[2] Jingdong Luo,[2] Sei-Hum Jang,[2] Alex K.-Y. Jen,[2] and Alan X. Wang[1,*]

[1]*School of Electrical Engineering and Computer Science Oregon State University, Corvallis, Oreton 97330, USA*
[2]*Department of Materials Science & Engineering, University of Washington, Seattle, Washington 98195, USA*
[*]*wang@eecs.oregonstate.edu,*

Abstract: The enhanced optical nonlinearity enabled by localized plasmonic fields has been well studied for all-optical switching processing (AOSP) devices for future optical communication systems. In this work, plasmonic photonic crystals with a nonlinear polycarbonate/polymethine blend cladding layer are designed to enhance the third harmonic generation (THG) at the telecom wavelengths (~1550 nm). Due to the presence of he two-dimensional (2-D) gold nano-patch arrays with improved Q-factor and high local fields, more than 20 × of enhanced THG signals in the hybrid organic-plasmonic nanostructure are experimentally observed. The enhanced THG in the hybrid organic-plasmonic materials suggested that such extraordinary nonlinear effects can be used for AOSP devices and wavelength conversion.

References and links

1. A. Martínez, J. Blasco, P. Sanchis, J. V. Galán, J. García-Rupérez, E. Jordana, P. Gautier, Y. Lebour, S. Hernández, R. Spano, R. Guider, N. Daldosso, B. Garrido, J. M. Fedeli, L. Pavesi, and J. Martí, "Ultrafast all-optical switching in a silicon-nanocrystal-based silicon slot waveguide at telecom wavelengths," Nano Lett. **10**(4), 1506–1511 (2010).
2. V. R. Almeida, C. A. Barrios, R. R. Panepucci, and M. Lipson, "All-optical control of light on a silicon chip," Nature **431**(7012), 1081–1084 (2004).
3. C. Koos, P. Vorreau, T. Vallaitis, P. Dumon, W. Bogaerts, R. Baets, B. Esembeson, I. Biaggio, T. Michinobu, F. Diederich, W. Freude, and J. Leuthold, "All-optical high-speed signal processing with silicon–organic hybrid slot waveguides," Nat. Photonics **3**(4), 216–219 (2009).
4. M. Hochberg, T. Baehr-Jones, G. Wang, M. Shearn, K. Harvard, J. Luo, B. Chen, Z. Shi, R. Lawson, P. Sullivan, A. K. Y. Jen, L. Dalton, and A. Scherer, "Terahertz all-optical modulation in a silicon-polymer hybrid system," Nat. Mater. **5**(9), 703–709 (2006).
5. J. I. Dadap, J. Shan, K. B. Eisenthal, and T. F. Heinz, "Second-harmonic rayleigh scattering from a sphere of centrosymmetric material," Phys. Rev. Lett. **83**(20), 4045–4048 (1999).
6. M. Kauranen and A. V. Zayats, "Nonlinear plasmonics," Nat. Photonics **6**(11), 737–748 (2012).
7. W. Cai, A. P. Vasudev, and M. L. Brongersma, "Electrically controlled nonlinear generation of light with plasmonics," Science **333**(6050), 1720–1723 (2011).
8. W. Wenseleers, F. Stellacci, T. Meyer-Friedrichsen, T. Mangel, C. A. Bauer, S. J. K. Pond, S. R. Marder, and J. W. Perry, "Five orders-of-magnitude enhancement of two-photon absorption for dyes on silver nanoparticle fractal clusters," J. Phys. Chem. B **106**(27), 6853–6863 (2002).
9. S. Palomba, M. Danckwerts, and L. Novotny, "Nonlinear plasmonics with gold nanoparticle antennas," J. Opt. A, Pure Appl. Opt. **11**(11), 114030 (2009).
10. M. Abb, P. Albella, J. Aizpurua, and O. L. Muskens, "All-optical control of a single plasmonic nanoantenna-ITO hybrid," Nano Lett. **11**(6), 2457–2463 (2011).
11. C. Lu, X. Hu, Y. Zhang, Z. Li, H. Yang, and Q. Gong, "Large Nonlinearity enhancement of Ag/MEH-PPV nanocomposite by surface plasmon resonance at 1,550 nm," Plasmonics **7**(1), 159–165 (2012).
12. H. B. Liao, R. F. Xiao, H. Wang, K. S. Wong, and G. K. L. Wong, "Large third-order optical nonlinearity in Au: TiO_2 composite films measured on a femtosecond time scale," Appl. Phys. Lett. **72**(15), 1817 (1998).
13. S. Chen, W. Wong, Y. Pun, K. Cheah, and G. Li, "Surface plasmon-enhanced third harmonic generation from gold–polymer hybrid plasmonic crystal," Adv. Opt. Mater. **1**(7), 522–526 (2013).
14. D. J. Ironside and J.-T. Shen, "Orders of magnitude enhancement of optical nonlinearity in subwavelength metal-nonlinear dielectric gratings," Appl. Phys. Lett. **102**(2), 021907 (2013).

15. G. A. Wurtz and A. V. Zayats, "Nonlinear surface plasmon polaritonic crystals," Laser Photon. Rev. **2**(3), 125–135 (2008).
16. X. Yang, A. Ishikawa, X. Yin, and X. Zhang, "Hybrid photonic-plasmonic crystal nanocavities," ACS Nano **5**(4), 2831–2838 (2011).
17. A. Scarpaci, A. Nantalaksakul, J. M. Hales, J. D. Matichak, S. Barlow, M. Rumi, J. W. Perry, and S. R. Marder, "Effects of dendronization on the linear and third-order nonlinear optical properties of bis (thiopyrylium) polymethine dyes in solution and the solid state," Chem. Mater. **24**(9), 1606–1618 (2012).
18. Z. Li, Y. Liu, H. Kim, J. M. Hales, S. H. Jang, J. Luo, T. Baehr-Jones, M. Hochberg, S. R. Marder, J. W. Perry, and A. K.-Y. Jen, "High-optical-quality blends of anionic polymethine salts and polycarbonate with enhanced third-order non-linearities for silicon-organic hybrid devices," Adv. Mater. **24**(44), OP326–OP330 (2012).
19. M. Grande, M. A. Vincenti, T. Stomeo, G. Morea, R. Marani, V. Marrocco, V. Petruzzelli, A. D'Orazio, R. Cingolani, M. De Vittorio, D. de Ceglia, and M. Scalora, "Experimental demonstration of a novel bio-sensing platform via plasmonic band gap formation in gold nano-patch arrays," Opt. Express **19**(22), 21385–21395 (2011).
20. B. D. Lucas, J.-S. Kim, C. Chin, and L. J. Guo, "Nanoimprint lithography based approach for the fabrication of large-area, uniformly oriented plasmonic arrays," Adv. Mater. **20**(6), 1129–1134 (2008).
21. H. Raether, Surface Polaritons on Smooth and Rough Surfaces and on Gratings, Springer-Verlag, Berlin (1988).
22. A. Christ, T. Zentgraf, J. Kuhl, S. G. Tikhodeev, N. A. Gippius, and H. Giessen, "Optical properties of planar metallic photonic crystal structures: experiment and theory," Phys. Rev. B **70**(12), 125113 (2004).
23. B. Luk'yanchuk, N. I. Zheludev, S. A. Maier, N. J. Halas, P. Nordlander, H. Giessen, and C. T. Chong, "The Fano resonance in plasmonic nanostructures and metamaterials," Nat. Mater. **9**(9), 707–715 (2010).
24. R. M. Bakker, A. Boltasseva, Z. Liu, R. H. Pedersen, S. Gresillon, A. V. Kildishev, V. P. Drachev, and V. M. Shalaev, "Near-field excitation of nanoantenna resonance," Opt. Express **15**(21), 13682–13688 (2007).
25. F. Ren, X. Wang, and A. Wang, "Thermo-optic modulation of plasmonic bandgap on metallic photonic crystal slab," Appl. Phys. Lett. **102**(18), 181101 (2013).
26. R. Boyd, Nonlinear Optics, Ch. 2, Academic Press (1992).
27. B. Corcoran, C. Monat, C. Grillet, D. J. Moss, B. J. Eggleton, T. P. White, L. O'Faolain, and T. F. Krauss, "Green light emission in silicon through slow-light enhanced third-harmonic generation in photonic-crystal waveguides," Nat. Photonics **3**(4), 206–210 (2009).

1. Introduction

In recent years, considerable efforts have been devoted to developing photonic materials that exhibit large nonlinearity and ultrafast response at 1550 nm for all-optical switching processing (AOSP) devices that can be used in future optical communication systems [1–4]. One of the most effective approaches to enhance the effective nonlinearity is through plasmonic effects, which arise from collective free electron motion near a noble metal surface. Surface-plasmon-enhanced nonlinear optical effects have been extensively investigated for nonlinear scattering, second harmonic generation (SHG), third harmonic generation (THG), two-photon absorption, four-wave mixing, AOSP and modulation [5–10]. Noble metal nanostructures have been combined with dielectric materials to generate even stronger nonlinear effects at 1550 nm. For example, metallic nanoparticle-doped nanocomposites and hybrid dielectric-plasmonic photonic crystals have been demonstrated recently [11,12]. However, this approach has several intrinsic drawbacks such as limited tunability of resonant wavelengths, large optical loss, and relatively small volume of hot spots. Compared to nanoparticles, metallic photonic crystals can couple light into surface plasmon polariton (SPP) Bloch modes, which significantly enhance the nonlinear light-matter interaction [13–16]. Therefore, it is important to effectively combine plasmon-active photonic crystals with dielectric materials that already have large nonlinear optical susceptibility at telecom wavelengths.

Oganic materials have been well studied for AOSP devices exhibiting ultra-fast third-order nonlinear optical responses, as well as low linear and nonlinear optical absorption [4, 8]. Among these organic functional materials, polymethine dyes are good candidates due to their highly delocalized π-electrons along the conjugated backbone [17,18]. Previously, an enhanced THG efficiency (3 ×) of a conjugated polymer on gold (Au) nanodisc/indium-tin-oxide (ITO) plasmonic photonic crystals has been demonstrated [13]. However, the enhancement is still quite low, and a relatively high threshold energy (> 2 μJ) from the pulsed laser was required for the THG emission. In addition, the 2-D nanodisc array suffers a low Q-factor, which is not suitable for practical AOSP devices.

In this work, we report the optical design, device fabrication, and experimental characterization of an organic-plasmonic hybrid nanostructure based on high-Q Au nanopatch

arrays infiltrated with a polymethine-based polymer to enhance the intensity of third-order harmonic generation. Numerical simulations based on finite-element analysis demonstrated localized SPPs from the two-dimensional (2-D) Au nano-patch arrays inside the polymer layer. Quantitative measurements of the THG intensity indicate that the hybrid nanostructure platform provides 20 × higher THG emission, which is significantly greater than that of the previously work [13]. In addition, the threshold of the energy from the incident pulsed laser is as low as 15 pJ.

2. Theoretical investigation of surface-plasmon-enhanced THG emission

The device structure is schematically shown in Fig. 1(a), which consists of 2-D arrays of Au patches on top of a glass substrate coated by a polymer thin film. In these hybrid organic-plasmonic devices, polymer(AJBC 1725) based on an anionic polymethine salt was used as the nonlinear medium to provide the THG effect. By careful structural optimization, AJBC 1725 shows excellent compatibility with the amouphous polycarbonate host polymer to form high optical quality composite films, which has very large third order nonlinear susceptibility, low optical loss, and excellent optical power handling capability [17]. We chose 2-D nano-patch arrays as the plasmonic resonator due to the symmetry of the structure. The device is insensitive to the angle of polarization within the plane parallel to the Au patch surface, which is favorable as a resonator over 1-D nanowire arrays that are polarization-dependent [19, 20]. The geometric dimensions are shown in Fig. 1(a), where the periodicities $p_x = p_y = 891$ nm, and the gap size between any two adjacent patches $g = 100$ nm. The thickness of the Au and polymer is designed at 100 nm and 1 μm respectively, as shown in Fig. 1(b).
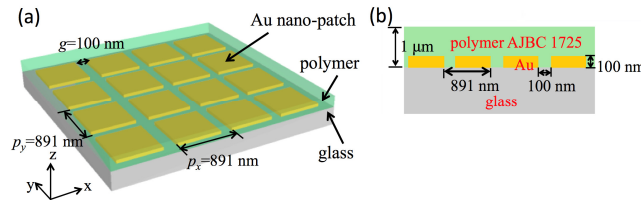

Fig. 1. (a)Sketch of the 2D gold nano-patch arrays on a glass substrate. The top layer is the nonlinear optical polycarbonate composite films doped with 50 wt% AJBC 1725(not to scale) (b) the cross-sectional view of the device structure.
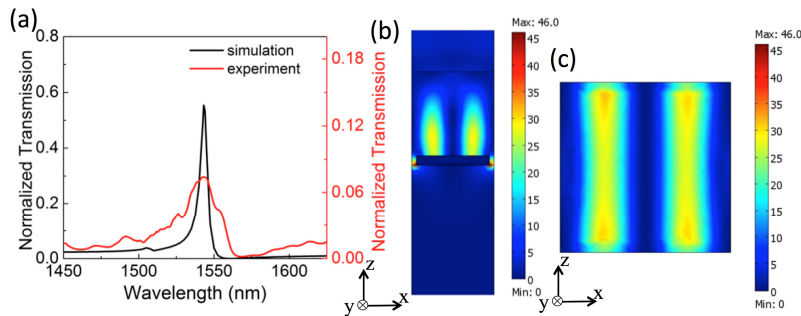

Fig. 2. The simulated (black) and experimental (red) transmission spectra are shown in (a). The intensity distribution of 2D periodic gold arrays for normally incident x-polarized E-field (b) from the cross-sectional view (c) from the top view (100 nm from the Au surface).

The electrical field enhancement and the optical transmission were theoretically investigated by conducting a three-dimensional (3-D) finite element simulation using the RF module within Comsol 3.5a. A plane wave was used as the excitation light with electric field polarized along the x-axis and a periodic boundary condition was applied in the simulation. Under normal incident, the excitation of SPPs with infinitely thick polymer is described by the zero-order relation [21]

$$\lambda_0 = n_{spp}p, \quad \text{with} \quad n_{spp} = \text{Re}\sqrt{\left(\frac{\varepsilon_{Au}\varepsilon_d}{\varepsilon_{Au} + \varepsilon_d}\right)} \tag{1}$$

The wavelength (λ_0) of the SPP is determined by the permittivities of the polymer (ε_d) and Au (ε_{Au}), and the periodicity of the 2-D patches (p) in Eq. (1). For Au nanopatch arrays with a thickness of 1μm, the polymer permittivity ε_d must be modified by the effective index of the fundamental waveguide mode, which is slightly smaller than the refractive index of the polymer AJBC 1725 of 1.8 measured by ellipsometry. At the near infrared wavelengths between 1400 nm and 1800 nm, a strongly asymmetric Fano resonance centered at 1543 nm was observed from the simulated wavelength range, as shown in Fig. 2(a). The discrete guided modes induced by the Bragg-grating-modulated SPPs couple to the broadband resonance in the narrow slits, resulting in strongly asymmetric resonances with a sharp bandgap [22,23]. A minimum transmission state at 1558 nm is shown in the transmission spectrum, which is a clear indication of the formation of the plasmonic bandgap. From the transmission spectrum, the Q-factor was determined to be as high as 257.

Figure 2(b) and 2(c) show the intensity distribution $|E/E_0|^2$ (where E_0 is the peak electric field of the incident light) associated with the SPPs at the Au-polymer interface of 1543 nm from the cross sectional view and the top view, respectively. Enhanced electric fields are located over the surface of the gold array, and the maximum enhancement factor of intensity $|E/E_0|^2$ is as high as 46. In a typical nanoplasmonic system, the field localization of a nanoantenna usually concentrates in a "hot spot" with the volume of a few cubic nanometers in the gap region [24], which limits the overall enhancement. However, the concentrated electric field in the 2D Au nanopatch array covers almost the entire Au patch surface and extends deeply into the polymer layer, resulting in a relatively uniform electric field enhancement over a large volume.

3. Device fabrication

Polymethine dye AJBC1725 was prepared in our previous work [18]. The polymethine dyes were mixed with APC (50% w/w) to prepare a guest-host polymer composite, then dissolved in dibromomethane with a concentration of ~5 wt%. Figure 3(a) shows the photograph of a spin-coated polymer thin film on a glass cover slide and has a thickness of ~1 μm.
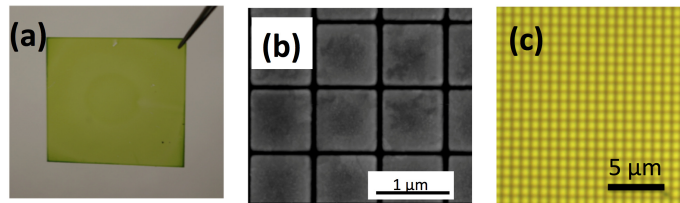

Fig. 3. (a) A representative photograph of the nonlinear polymer thin film on a glass substrate (not to scale) (b) The SEM image of the plasmonic structure after FIB process, showing highly ordered nano-patch arrays (c) The optical image of the plasmonic structure.

We started the fabrication of the plasmonic structure by depositing a 100 nm Au thin film on a glass substrate (index is 1.5023) by thermal evaporation with a deposition rate of 8 Å/Sec. The 2-D Au nano-patch arrays were patterned by focused-ion beams (FIB), with a gallium ion current of 14.5 pA and a dose of 5 mC/cm^2. A scanning electron microscopy (SEM) image of the 2-D nano-patch arrays after the FIB milling is shown in Fig. 3(b), which indicates that highly ordered 2-D arrays of nano-patches were formed with slightly rounded corners (curvature less than 15 nm). A thin film (1 μm) of nonlinear polymer composite was spin-coated on top of the Au layer to form the hybrid plasmonic-organic structure at 1900 rpm for 120 s. The optical image of the fabricated plasmonic-organic device is shown in Fig. 3(c). In order to compare the THG efficiency, a control device was also fabricated, with 1 μm polymer on top of a 100 nm Au thin film without any plasmonic structure.

4. Optical transmission and THG measurement

The experiment setup of the optical transmission measurement has been discussed in the previous work [25]. From the transmission spectrum in Fig. 2(a), an asymmetric Fano resonance peak is shown on the measured wavelength range, with the resonant peak centered at 1543 nm and a full width half maximum of 22 nm. Therefore, the measurement showed a Q-factor of 70.1, which is less than the results of the simulation mentioned previously. The enlarged bandgap of the Fano resonance and the reduced Q-factor are possibly due to the non-ideal Au film quality, fabrication defects, and the imperfect beam collimation.

The experimental setup for observing THG signals from the plasmonic-organic device is shown in Fig. 4(a). A fiber-based femtosecond laser (Calmar Laser, FPL-03CFF) was launched to pump the the polymer-Au hybrid plasmonic device with a repetition frequency of 20 MHz. The output light was collimated by a 40 × objective lens (NA = 0.65). A dichroic mirror was used to reflect the pump laser centered at 1550 nm, while also allowing the transmission of the THG wavelengths centered at 517 nm. The reflected beam was focused by a 100 × objective lens (NA = 0.90). The plasmonic-organic sample was mounted at the focal plane of the objective lens on a three-dimensional translation stage. After focusing, the diameter of the spot size of the pump laser was ~8 μm. The THG emission was imaged by a colored CCD camera (Thorlabs, DCC1645C) in the far field after filtering the pump laser using a bandpass filter (Thorlabs, FB520-10). The captured high-resolution images from the CCD in Fig. 4(b) and 4(c) compare qualitatively the THG emission from the polymer with the plasmonic structures and from the polymer without the plasmonic structure (a pure gold thin film, control device). The qualitative comparison indicates that the polymer with plasmonic structure has a much greater THG efficiency ($\eta = I_{THG}/I_{pump}$) at frequency $\omega_{THG} = 3\omega_0$, which is due to the electric field enhancement of the surface plasmon resonance at the organic-plasmonic structure.
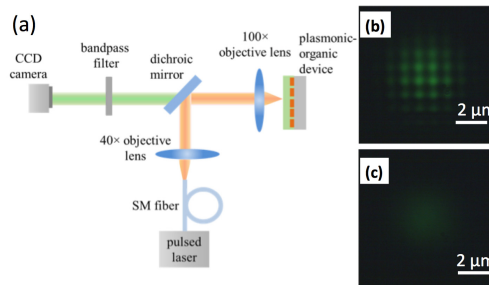

Fig. 4. (a) The experimental setup of the THG signal imaging system for the devices. (b) The captured THG signal intensities from the plasmonic-organic structure (c) The captured THG intensities from polymer without the plasmonic structure.

Further study was focused on the quantitative measurement of the intensities of THG signals from the hybrid organic-plasmonic device. The CCD camera was replaced by a photomultiplier tube, which was used to measure the intensity of the THG signals. A fiber-based tunable filter was used to manually select the wavelength of the pumping light with a narrow spectral bandwidth of 3.2 nm, tuning the output wavelength from 1532 nm to 1565 nm. Figure 5(a) shows the THG response by tuning the wavelengths of the fs-laser. The measured results show that the hybrid organic-plasmonic structure provides as high as 21.6 × the enhancement of the response compared to that of the control device. The peak of the enhancement factor in the inset figure in Fig. 5(a) matches the resonant peak of the measured spectrum, which confirms the enhancement from the localized SPPs at the Au-polymer interface.
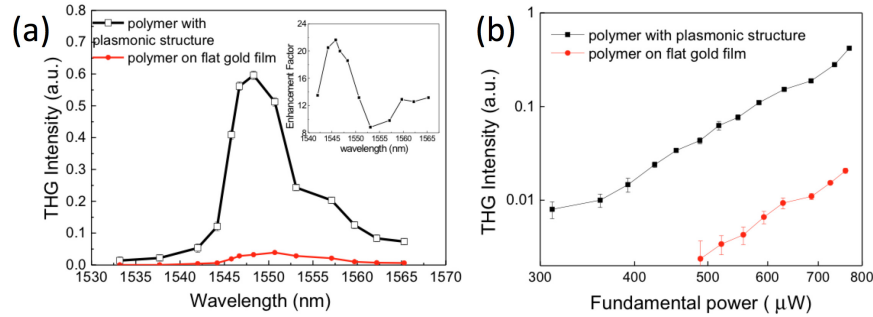
Fig. 5. (a) The THG wavelength dependence of the nonlinear optical polymer composite with and without plasmonic structure respectively. The inset figure shows the enhancementment factors as a function of wavelengths. (b) The THG power dependence of the polymer with and without plasmonic structure, respectively.

The dependence of the THG intensity with respect to the pumping power at 1550 nm was also investigated in this work. A fiber-based attenuator was connected with the output of the femtosecond laser in order to adjust the intensity of the pumping light coupled into the system. The THG (electric field intensity $I_{3\omega}$, frequency 3ω) from a fundamental light (electric field intensity I_ω, frequency ω) is expected to have a cubic dependence on the fundamental power in the measurement for perfect phase matching and maximum mode overlap between the fundamental mode and the third harmonic wavevectors [26,27]. The power dependence of THG is plotted in Fig. 5(b). The THG was much stronger in the polymer with plasmonic structures compared with that of the control device within the measured power range. Due to the presence of the SPPs at the polymer/Au interfaces, the average enhancement factor reaches as high as 20 × . THG was observed through the entire measurement range from 312 μW to 773 μW in the hybrid plasminic-organic structure. With a repetition rate at 20 MHz, the pulsed energy for the THG emission threshold is as low as 15 pJ, which is reduced by a factor of over 10^5 compared to the previously reported results [13]. For the control device, the THG emission could only be observed above the threshold of the fundamental power of 485 μW. Therefore, it can be concluded from the power-dependence measurement that the THG from the organic-plasmonic hybrid structure is considerably higher than that from a pure polymer thin film.

5. Summary

In conclusion, we have designed and fabricated a hybrid plasmonic-organic nanostructure to enhance the THG efficiency at the telecom wavelengths of 1550 nm. Numerical simulations show that the 2D plasmonic structure creates a large-volume optical field enhancement throughout the bulk polymer, which is proved by the qualitative comparison of the THG intensity from the images of a CCD camera. Further experiments show that over 20 × enhancement factor of the THG conversion efficiency could be observed in our nanostructure due to the electric field localization at the SPP resonant wavelengths. This hybrid plasmonic-organic nanostructure opens a new route for future AOSP devices.

Acknowledgment